

ASM Handbook Volume 22 – Modeling and Simulation: Processing of Metallic Materials

9. Simulation of PM processes

9.C. Metal Powder Injection Molding

Seokyoung Ahn¹, Seong-Taek Chung², Seong Jin Park³, and Randall M. German⁴

¹ Department of Mechanical Engineering, The University of Texas-Pan American, 1201 W University Dr., Edinburg, TX 78539, USA

² CetaTech, Inc., TIC 296-3, Seonjin-Ri, Sacheon-Si, Kyongnam, 664-953, Korea

³ Center for Advanced Vehicular Systems, Mississippi State University, 200 Research Blvd., Starkville, MS 39759, USA

⁴ College of Engineering, San Diego State University, 5500 Campanile Drive, San Diego, CA 92182-1326, USA

Introduction

Plastics formed by injection molding are used everywhere, because of the low overall cost in a high level of shape complexity. Powder injection molding (PIM) builds on the long recognized success of plastic molding by using a high particle content thermoplastic as feedstock. The steps in PIM involve first mixing selected small powders (usually smaller than 20 μm) and polymer binders. The particles are small to aid in sintering densification and often have near spherical shapes to improve flow and packing. The thermoplastic binders are mixtures of waxes, polymers, oils, lubricants, and surfactants. When molten, the binder imparts viscous flow characteristics to the mixture to allow filling of complex tool geometries. A favorite binder system relies on a mixture of paraffin wax and polypropylene, with a small quantity of stearic acid. The combination of powder and binder that works best gives a paste with about the same consistency as toothpaste, with no voids; this often leads to a formulation near 60 volume percent powder and 40 volume percent binders. This mixture is heated in the molding machine, rammed into a cold mold, and when the binder freezes in the mold, the component is ejected. Next, the binder is removed by heat and solvents (some of the binders are water soluble) and the remaining 60% dense powder structure is then sintered to near-full density. The product may be further densified, heat treated, machined, or plated. The sintered compact has the shape and precision of an injection molded plastic, but is capable of performance levels unattainable with polymers. Almost half of all PIM is applied to stainless, steels, but a

wide variety of compositions are in production [1].

The equipment used for shaping the compact is the same as used for plastic injection molding, so software for molding machine control is the same as found in plastics. Most molding machines fill a die through a gate from a pressurized and heated barrel (the barrel and gate are connected by a nozzle and runner). A plunger or reciprocating screw generates the pressure needed to fill the die. Computer simulations used for mold filling in plastics are not directly useful for powder injection molding, since inertia, thermal conductivity, and powder-binder separation are new concerns with PIM feedstock. The feedstock enters the barrel as cold granules and during compression to remove trapped air it is heated above the binder melting temperature. Because the feedstock is hot and the die is cold, filling must be accomplished in a split second to avoid premature freezing. After filling the die, packing pressure is maintained on the feedstock during cooling to eliminate shrinkage voids. After sufficient cooling, the hardened compact is ejected and the cycle repeated. It is common to have multiple cavities (4 or more) and cycle times of 15 s, so production rates of 16 parts per minute are often observed.

The PIM process is practiced for a very wide range of materials, including most common metal, many ceramics, and cemented carbides. The largest uses are in metal powder injection molding, denoted as MIM. Other variants are CIM for ceramic injection molding and CCIM for cemented carbide injection molding.

Simulations used for plastics have been applied to PIM, but the high solid content often makes for differences that are ignored in the plastic simulations. Several situations demonstrate the problems, such as powder-binder separation at weldlines, high inertial effects such as in molding tungsten alloys, and rapid heat loss such as in molding copper and aluminum nitride. Also, powder-binder mixtures are very shear rate sensitive. Thus, the computer simulations to support molding build from the success demonstrated in plastics, but adapt those concepts in new customized PIM simulations for filling, packing, and cooling.

Theoretical Background and Governing Equations

A typical injection molded component has a thickness much smaller than the overall largest dimension. A typical wall thickness is in the 1 to 3 mm range, while the longest dimension might range near 25 mm with an overall mass near 10 g. There is much variation, but these values offer a glimpse at the typical components [2]. In molding such components, the molten powder-binder feedstock mixture is highly viscous. As a result, the Reynolds number (a dimensionless number characterizing a ratio of inertia force to viscous force) is low and the flow is modeled as a creeping flow with lubrication, as treated with the

Hele-Shaw formulation. With the Hele-Shaw model, the continuity and momentum equations for the melt flow in the injection molding cavity are merged into a single Poisson equation in terms of the pressure and fluidity. Computer simulation is usually based on a 2.5-dimensional approach because of the thin wall and axial symmetry. But the Hele-Shaw model has its limitations and cannot accurately describe three-dimensional (3D) flow behavior in the melt front, which is called fountain flow, and special problems arise with thick parts with sudden thickness changes, which cause race-track flow.

Nowadays, several 3D computer aided engineering simulations exist that successfully predict conventional plastic advancement and pressure variation with changes in component design and forming parameters [3]. For PIM 3D simulation, Hwang and Kwon [4] developed a filling simulation with slip using an adaptive mesh refinement technique to capture the large deformation of the free surfaces, but this is computationally intensive [4-7], so further research is moving toward simplified solution routes [3]. In this section, we will focus on the axisymmetric 2.5-dimensional approach rather than a full 3D approach, because the 2.5-dimensional approach is more robust and better accepted by industry. The post-molding sintering simulation is described in the earlier press-sinter simulation.

Filling Stage

Powder injection molding involves a cycle that repeats every few seconds. At the start of the cycle, the molding machine screw rotates in the barrel and moves backward to prepare molten feedstock for the next injection cycle while the mold closes. The mold cavity fills as the reciprocating screw moves forward, acting as a plunger, which is called the filling stage. During the filling stage, a continuum approach is used to establish the system of governing equations as follows:

- *Mass and momentum conservation:* With the assumption of incompressible flow, the mass conservation, also called continuity equation, is expressed as,

$$\frac{\partial u}{\partial x} + \frac{\partial v}{\partial y} + \frac{\partial w}{\partial z} = 0 \quad (1)$$

where x , y , and z are Cartesian coordinates and u , v , and w are corresponding orthogonal velocity components. As for the momentum conservation, with lubrication and the Hele-Shaw approximation, the Navier-Stokes equation is modified for molten feedstock during filling stage as follows [8-9],

$$\begin{aligned}\frac{\partial P}{\partial x} &= \frac{\partial}{\partial z} \left(\eta \frac{\partial u}{\partial z} \right) \\ \frac{\partial P}{\partial y} &= \frac{\partial}{\partial z} \left(\eta \frac{\partial v}{\partial z} \right) \\ \frac{\partial P}{\partial z} &= 0\end{aligned}\quad (2)$$

where P is the pressure, z is the thickness, and η is the viscosity of PIM feedstock. By combining Equations (1) and (2) with integration in z -direction (thickness direction) gives,

$$\frac{\partial}{\partial x} \left(S \frac{\partial P}{\partial x} \right) + \frac{\partial}{\partial y} \left(S \frac{\partial P}{\partial y} \right) = 0 \quad (3)$$

where

$$S \equiv \int_{-b}^b \frac{z^2}{\eta} dz \quad (4)$$

Equation (3) is the flow governing equation for the filling stage. This is exactly the same form of steady-state heat conduction equation obtained by substituting temperature T into P and thermal conductivity k into S . In this analogy, S is the flow conductivity or fluidity. As a simple interpretation of this flow governing equation, molten PIM feedstock flows from the high pressure region to the low pressure region, and the speed of flow depends on the fluidity S . During the calculation, the fluidity increases as the thickness of component increases and the viscosity of PIM feedstock decrease for feedstock cooling. After obtaining the pressure field, the velocity components u and v are obtained by integrating Equation (2) in the z -direction (thickness direction).

- *Energy Equation:* In accordance with the lubrication and Hele-Shaw approximations during the filling stage, the energy equation is simplified as follows:

$$\rho C_p \left(\frac{\partial T}{\partial t} + u \frac{\partial T}{\partial x} + v \frac{\partial T}{\partial y} \right) = k \frac{\partial^2 T}{\partial z^2} + \eta \dot{\gamma}^2 \quad (5)$$

where ρ is the molten PIM feedstock's density, C_p is the molten PIM feedstock's specific heat, and $\dot{\gamma} = \sqrt{(\partial u / \partial z)^2 + (\partial v / \partial z)^2}$ is generalized shear rate and k is the thermal conductivity of the feedstock.

In addition, we need a constitutive relation to describe the molten PIM feedstock's response to its flow environment during cavity filling, which requires a viscosity model. Several viscosity models for

polymers containing high concentrations of particles are available. Generally they include temperature, pressure, solids loading, and shear strain rate and selected models will be introduced later in this chapter. The selection of a viscosity model depends on the desired simulation accuracy over the range of processing conditions, such as temperature and shear rate, as well as access to the experimental procedures used to obtain the material parameters.

Once we have the system of differential equations from continuum-based conservation laws and the constitutive relations for analysis of the filling stage, then we need boundary conditions. Typical boundary conditions during the filling stage are as follows:

- boundary conditions for flow equation: flow rate at injection point, free surface at melt-front, no slip condition at cavity wall and
- boundary conditions for energy equation: injection temperature at injection point, free surface at melt-front, mold-wall temperature condition at cavity wall.

Note that the only required initial condition is the flow rate and injection temperature at the injection node, which is one of the required boundary conditions.

For a more rigorous approach during the filling stage, a few efforts have invoked a full 3D model, and have included fountain flow, viscoelastic constitutive models, slip phenomena, yield phenomena, and inertia effects in governing equations and interface [3, 5-6, 10].

Packing Stage

When mold filling is nearly completed, the packing stage starts. This precipitates a change in the ram control strategy for the injection molding machine, from velocity control to pressure control, which is called the switch-over point. As the cavity nears filling, the pressure control ensures full filling and pressurization of the filled cavity prior to freezing of the gate. It is important to realize the packing pressure is used to compensate for the anticipated shrinkage in the following cooling stage. Feedstock volume shrinkage results from the high thermal expansion coefficient of the binder, so on cooling there is a measurable contraction. By appropriate pressurization prior to cooling, then after the gate freezes the component shrinks sufficiently that there are no sink marks (too low a packing pressure) and no difficulty with ejection (too high a packing pressure).

For the analysis of the packing stage, it is essential to include the effect of melt compressibility.

Consideration is given to the melt compressibility using a dependency of the specific volume on pressure and temperature, leading to a feedstock specific pressure-volume-temperature (pVT) relationship, or the equation of state. Several models are available to describe the pVT relation of PIM feedstock, such as the 2-domain modified Tait model and IKV model. These models predict an abrupt volumetric change for

both semi-crystalline polymers used in the binder and the less abrupt volume change for amorphous polymers used in the binder.

With the proper viscosity and pVT models, the system of governing equation for the packing stage based on the continuum approach is as follows:

- *Mass conservation:* The continuity equation of compressible PIM feedstock is expressed as,

$$\frac{\partial \rho}{\partial t} + \frac{\partial(\rho u)}{\partial x} + \frac{\partial(\rho v)}{\partial y} + \frac{\partial(\rho w)}{\partial z} = 0 \quad (6)$$

with the assumption that pressure convection terms may be ignored in the packing stage this becomes:

$$\kappa \frac{\partial p}{\partial t} - \beta \left(\frac{\partial T}{\partial t} + u \frac{\partial T}{\partial x} + v \frac{\partial T}{\partial y} \right) + \left(\frac{\partial u}{\partial x} + \frac{\partial v}{\partial y} \right) = 0 \quad (7)$$

where κ is the isothermal compressibility coefficient of the material ($\partial \rho / \rho \partial p$) and β measures the volumetric expansivity of the material ($\partial \rho / \rho \partial T$). Those are easily calculated from the equation of state. Note that the same momentum conservation is used as Equation (2) regardless of the material to be considered as compressible or not.

- *Energy Equation:* The energy equation is derived as,

$$\rho C_p \left(\frac{\partial T}{\partial t} + u \frac{\partial T}{\partial x} + v \frac{\partial T}{\partial y} \right) = k \frac{\partial^2 T}{\partial z^2} + \eta \dot{\gamma}^2 + \beta T \frac{\partial p}{\partial t} \quad (8)$$

That is, the shear rate for the compressible case in packing is for practical purposes the same as for the filling phase.

Typical initial and boundary conditions during packing stage are as follows:

- initial conditions: pressure, velocity, temperature, and density from the results of the filling stage analysis,
- boundary conditions for equations of mass and momentum conservations: prescribed pressure at injection point, free surface at melt-front, no slip condition at cavity wall, and
- boundary conditions for energy equation: injection temperature at injection point, free surface at melt-front, and mold-wall temperature condition at the cavity wall, which is interfaced with the cooling stage analysis.

Cooling Stage

Of the three stages in the injection molding process, the cooling stage is of greatest importance because it significantly affects the productivity and the quality of the final component. Cooling starts immediately upon the injection of the feedstock melt, but formally the cooling time is referred to as the time after the gate freezes and no more feedstock melt enters the cavity. It lasts up to the point of component ejection, when the temperature is low enough to withstand the ejection stress. In the cooling stage, the feedstock volumetric shrinkage is counteracted by the pressure decay until the local pressure drops to atmospheric pressure. Thereafter, the material shrinks with any further cooling, possibly resulting in residual stresses due to nonuniform shrinkage or mold constraints (which might not be detected until sintering). In this stage, the convection and dissipation terms in the energy equation are neglected since the velocity of a feedstock melt in the cooling stage is almost zero [11-13]. Therefore, the objective of the mold-cooling analysis is to solve only the temperature profile at the cavity surface to be used as boundary conditions of feedstock melt during the filling and packing analysis.

When the injection molding process is in steady-state, the mold temperature will fluctuate periodically over time during the process due to the interaction between the hot melt and the cold mold and circulating coolant. To reduce the computation time for this transient process, a 3D cycle-average approach is adopted for the thermal analysis to determine the cycle-averaged temperature field and its effects on the PIM component. Although the mold temperature is assumed invariant over time there is still a transient for the PIM feedstock [14], leading to the following features:

- *Mold Cooling Analysis:* Under this cycle-average concept, the governing equation of the heat transfer for injection mold cooling system is written as

$$\nabla^2 \bar{T} = 0 \quad (9)$$

where \bar{T} is the cycle-average temperature of the mold.

- *PIM Component Cooling Analysis:* Without invoking a flow field, the energy equation is simplified as

$$\rho C_p \frac{\partial \bar{T}}{\partial t} = k \frac{\partial^2 \bar{T}}{\partial z^2} \quad (10)$$

Typical initial and boundary conditions applied during the cooling stage are as follows:

- initial conditions: temperature as calculated from the packing stage analysis,

- boundary conditions - mold: interface input from the PIM feedstock cooling analysis, convection heat transfer associated with the coolant, natural convection heat transfer with air, and thermal resistance condition from the mold platen, and
- boundary conditions - component: interface input from the mold cooling analysis.

Note that the boundary conditions for the mold and PIM feedstock cooling are coupled to each other. More details on this are given in the Numerical Simulation section below.

For a more rigorous approach during the cooling stage, some researchers have included more than two different mold materials with flow analysis that includes the cooling channel details. This enables corresponding heat transfer analysis with any special cooling elements, such as baffles, fountains, thermal pin, or heat pipes [12].

Numerical Simulation

As far as the numerical analysis of injection molding is concerned, several numerical packages are already available for conventional thermoplastics. And one may try to apply the same numerical analysis techniques to PIM. However, the rheological behavior of a powder-binder feedstock mixture is significantly different from that of a thermoplastic. Hence, the direct application of methods developed for thermoplastics to PIM requires caution [4, 10]. Commercial software packages, including Moldflow (Moldflow Corp., Framingham, MA), Moldex3D (CoreTech System Co., Ltd., Chupei City, Taiwan), PIMsolver (CetaTech, Sacheon, Korea), and SIMUFLOW (C-Solutions, Inc., Boulder, CO) are available for PIM simulation. Further, several research groups have written customized codes, but generally these are not released for public use.

It is well known that powder-binder feedstock mixtures used in PIM exhibit a peculiar rheological feature known as wall slip [10, 15]. Therefore, a proper numerical simulation of the PIM process essentially requires a proper constitutive equation representing the slip phenomena of powder-binder feedstock mixtures [10, 14].

Filling and Packing Analysis

For numerical analysis of the filling and packing stages of PIM, both the pressure and energy equations must be solved during the entire filling and packing cycle. This is achieved using the finite element method for Equation (2) while a finite difference method is used in the z -direction (thickness), making use of the same finite elements in the x - y plane for solving Equation (3).

The finite difference method (FDM) is a relatively efficient and simple numerical method for solving

differential equations. In this method, the physical domain is discretized in the form of finite-difference grids. A set of algebraic equations is generated as the derivatives of the partial differential equations and are expressed by finite differences of the variable values at the grid points. The resulting algebraic equation array, which usually forms a banded matrix, is solved numerically. Generally, the solution accuracy is improved by reducing the grid spacing. However, since the FDM is difficult to apply to a highly irregular boundary or a complicated domain typical of injection molding, the use of this method has to be restricted to regular and simple domains, or used with the finite element method (FEM) as a FDM-FEM hybrid scheme [3].

The FEM has been excellent flexibility in treating complex geometries and irregular boundaries, which is a key advantage of this method. It requires discretizing the physical domain into several finite elements. The field variables are represented with shape functions and nodal values over each finite element. Using residual minimization techniques (or, equivalently, variational techniques) such as the Galerkin method, the governing equations are transformed into discretized forms [8, 9]. For three-dimensional simulation of injection molding, the resulting global matrix system from the algebraic equations is a typically large and sparse, which requires large memory space and processing time. The central processor use time may be estimated based on the number of elements in the meshes and the degrees of freedom (DOF) per node. In transient problems, a finite-difference expression for the time derivatives is typically used in conjunction with the finite-element discretization.

For the numerical analysis of the filling process of PIM, one has to solve both the pressure equation and energy equation during the entire filling cycle until the injection mold cavity is filled. A FEM method is employed to solve Equations (2) and (3) while FDM is used in thickness-wise (z-direction) making use of the same finite elements in the x-y plane [9].

Cooling Analysis

For the numerical analysis of the cooling process in PIM, the boundary element method (BEM) is widely used due to its advantage in reduction of the dimensionality of the solution. The BEM discretize the domain boundary rather than the interior of the physical domain. As a result, the volume integrals become surface integrals, then the number of unknowns, computation effort, and mesh generation are significantly reduced [3].

A standard boundary element method formulation for Equation (9) based on Green's second identity leads to the following:

$$\alpha T(\mathbf{x}) = \int_S \left[\frac{1}{r} \left(\frac{\partial T(\zeta)}{\partial n} \right) - T(\zeta) \left(\frac{1}{r} \right) \right] dS(\zeta) \quad (11)$$

Here \mathbf{x} and $\boldsymbol{\zeta}$ relate to the positional vector in the mold, $r = |\boldsymbol{\zeta} - \mathbf{x}|$, and α denotes a solid angle formed by the boundary surface. Equation (11) for two closed surfaces, such as defined by the component shape, leads to a redundancy in the final system of linear algebraic equations, so a modified procedure is used [16]. For circular hole, a special formulation is created based on the line-sink approximation. This approach avoids discretization of the circular channels along the circumference and significantly saves computer memory and time.

For the thermal analysis of a PIM component, the FDM is used with the Crank-Nicholson algorithm for time advancement. The mold and PIM component analyses are coupled with each other in boundary conditions so iteration is required until the solution converges.

Coupled Analysis between Filling, Packing, and Cooling Stages

The filling, packing, and cooling analyses are coupled to each other. When we analyze the filling and packing stages, we have the cavity wall temperature as a boundary condition for the energy equation. This cavity wall temperature is obtained from the cooling analysis. On the other hand, when we analyze the cooling stage, we have the temperature distribution of the powder-binder feedstock mixture in the thickness direction at the end of filling and packing as an initial condition for the heat transfer of powder-binder feedstock. This initial temperature distribution is obtained from the filling and packing analysis. Therefore, the coupled analysis among the filling, packing, and cooling stages might be made for accurate numerical simulation results [14].

Figure 1 shows typical procedure for computer simulation for powder injection molding process, which consists of three components; Input Data, Analysis, and Output Data. The quality of the Input Data is essential to success. The Pre-processor is a software tool used to prepare a geometric model and mesh for the component and mold; it includes –

1. material data for feedstock, mold, and coolant
2. processing conditions for filling, packing, and cooling processes.

Figure 2 shows one example of geometry modeling and mesh generation for a U-shape component, including the delivery system and cooling channels.

Experimental - Material Properties and Verification

Material Properties for Filling Stage

Successful simulation of the filling stage during PIM depends on measuring the material properties,

including density, viscosity, and thermal behavior. Among these, the viscosity of the PIM feedstock and its variation with temperature, shear rate, and solid volume fraction are special concerns [17-19]. The following procedure is an example of the method used to obtain these material properties. For this illustration, assume a spherical stainless steel powder in a wax-polymer binder.

- First, melt densities, heat capacities, and thermal conductivities of the binder and feedstock are required. This is attained using a helium pycnometer, differential scanning calorimeter, and laser flash thermal conductivity device.
- Second, the transition temperature for the feedstock is measured, again using differential scanning calorimetry.
- Third, the binder viscosity is measured and fit to a model. For the characterization of the binder viscosity, a rotational-type rheometer is widely used due to relatively low viscosity of the wax. From the measured slow strain rate viscosity data, binder viscosity is obtained by curve fitting to a Newtonian binder viscosity model (η_b) with temperature (T) dependency:

$$\eta_b = B_b \exp\left(\frac{T_{b,b}}{T}\right) \quad (12)$$

where B_b is the constant amplitude and $T_{b,b}$ is an Arrhenius type coefficient, also called as the reference temperature.

- Fourth, the feedstock viscosity is measured versus key parameters. The rheological behavior of the feedstock is measured by capillary rheometry. The slip characteristics of the PIM feedstock is determined using three different capillary dies with different the length-to-diameter ratios [20]. By using high length-to-diameter ratio capillaries, the pressure loss correction, called Bagley's correction, is avoided. Rabinowitch's correction is extracted to obtain the true shear rate from the apparent shear rate for a non-Newtonian fluid, characteristic of the feedstock [10]. The variation of viscosity with temperature is determined by testing the feedstock at different temperature above the transition temperature. Such capillary measurements are typically carried out three times to confirm the repeatability of the data, giving a total of 27 tests - 3 different diameter dies, 3 different temperatures, and 3 replications.
- Fifth, the feedstock viscosity data are modeled using standard loaded polymer concepts. A concentrated powder-binder feedstock mixture has a yield strength with shear-thinning viscous behavior [15]. The modified-Cross model for viscosity as a function of the effective shear rate and temperature as expressed below is the most useful treatment:

$$\eta_m(\dot{\gamma}, T) = \frac{\eta_0}{1 + (\eta_0 \dot{\gamma} / \tau^*)^{1-n}} + \frac{\tau_y}{\dot{\gamma}} \quad (13)$$

where temperature enters the same as in Equation (12),

$$\eta_0 = B \exp(T_b / T). \quad (14)$$

In Equations (13) and (14), the subscript m indicates the powder-binder feedstock mixtures, while τ_0 , n , τ^* , B and T_b denote the zero shear rate viscosity, the power law exponent, the transition shear stress, the power law exponent, the transition stress, the constant amplitude and the reference temperature (absolute scale) for the Arrhenius temperature dependence. A term τ_y is added to the modified-Cross model for the yield stress [14, 21]. To introduce the slip phenomena, two models can be used:

Slip velocity model:

$$V_S = \alpha_1 \exp(\beta_1 T) \tau_w^{m_1} \quad (15)$$

Slip layer model:

$$\delta = \alpha_2 \exp(\beta_2 T) \tau_w^{m_2} \quad (16)$$

In Equations (15) and (16), the subscript 1 and 2 indicate the slip velocity and slip layer models, respectively, and α , β , and m are the material constants. Figure 3 illustrates the concept of the slip layer and slip velocity. All the material parameter for feedstock viscosity based on Equations (13) to (16) is obtained by curve fitting from the measured viscosity data.

Table 1 gives an example of the material properties used in the PIM filling stage simulation for a 316L stainless steel powder with a median particle size of 8.0 μm in a standard wax-polymer binder system at a solid volume of 53 %. Figure 4 demonstrates the importance of introducing slip phenomena into viscosity model for the above feedstock at 100°C. This plot shows the raw viscosity versus shear strain rate using three capillary diameters, and the collapse of those results into a single curve with the slip correction.

Material Properties for the Packing Stage

To simulate the packing stage, the Hele-Shaw flow of a compressible viscous melt of PIM feedstock under non-isothermal conditions is assumed. For this, the two-domain modified Tait model is adopted to describe the phase behavior of the feedstock [8]. A dilatometer is used to measure dimensional changes as a function of temperature and other variables and the results are extracted by curve fitting.

Table 2 and Figure 5 give one example of pvt material properties based on the following 2-domain modified Tait model for the packing stage simulation for the same stainless steel feedstock. For the solid-liquid phase:

$$\begin{aligned}
v(p, T) &= v_0(T) \left[1 - 0.0894 \ln \left(1 + \frac{p}{B(T)} \right) \right] + v_i(p, T) \\
v_0(T) &= b_1 + b_2 \bar{T} \\
B(T) &= b_3 \exp(-b_4 \bar{T}) \\
\bar{T} &= T - b_5 \\
v_i(p, T) &= b_7 \exp(b_8 \bar{T} - b_9 P)
\end{aligned} \tag{17}$$

with the transition temperature, T_g , which is calculated as $T_g(p) = b_5 + b_6 p$.

Material Properties for the Cooling Stage

For the cooling stage simulation, material properties of mold material and coolant need to be measured. Table 3 gives one example of the material properties for a typical H13 tool steel as the mold material with water as the coolant.

Verification

Verification of the simulation is a critical step prior to any effort to optimize a design based on simulations. This verification usually includes the validation of the model used in developing the software. To demonstrate the verification of the simulation tool through experiment, we selected the U-shaped test mold shown in Figure 2 with the stainless steel PIM feedstock reported above and a H13 mold. Three pressure transducers were used to compare the simulation results with the experimental data. The cavity thickness is 3 mm and the gate diameter is 1 mm. The coolant inlet temperature is 20°C, the inlet flow rate is 50 cm³/s, and the cooling time is 10 s, respectively, as summarized in Table 4.

Figure 6 describes some of the simulation results obtained using PIMsolver. Figure 6(a) shows the filling pattern, indicating how the mold cavity fills as a function of time with the slip-layer model. The filling time was 1.28 s. Figure 6(b) shows the average mold-temperature distributions on the upper and lower surfaces of the cavity from the cooling analysis results. The highest average temperature is 51°C and occurs at the base of the U and the lowest temperature is 34°C at the runner inlet. The mold wall temperature is not uniform and the difference between maximum and minimum values is 18°C. This variation is large enough to cause a significant difference in the solidification layer development during the packing stage. Therefore, one might expect the simulation to have a significant error in pressure prediction during the packing stage without consideration of the cooling effect. Figure 6(c) shows the distribution of the slip layer thickness at the end of filling. The predicted slip layer thickness is from 0.8 to 6.2 μm, which is less than the 8 μm median particle size. A high slip layer thickness becomes an insulator during cooling, resulting in non-uniform cooling and increased cooling time.

To examine the validation and importance of the slip phenomena and the coupled analysis between the filling/packing and cooling stages, the pressure traces were compared between simulation and experiment, as shown in Figure 7 using the three positions indicated in Figure 2. Figure 7 gives the pressure-time plot obtained from the experiment and simulation. The simulation results were obtained from the filling and packing analyses at a constant cavity wall temperature of 30°C without and with consideration of slip layer. As shown in Figures 7(a) and 7(b), the simulation results obtained with the slip layer provide a better fit to the experimental data. Without the slip correction there is an underestimation of the pressure. However, the simulation results with the slip correction continue to show significant deviations from experiment results. The results with the distributed mold wall temperature interfaced with the results from cooling analysis, as shown in Figure 7(c), explain this deviation. If we consider the cavity wall temperature distributions from the cooling analysis (coupled analysis), then that temperature enables the best agreement to the experimental results. This is because the constant mold wall temperature is lower than obtained from the cooling analysis, and the mold wall temperature is not uniform. In addition, the accuracy of pressure prediction at the end of the packing stage (about 4 s) is improved due to the difference in the development of solidification layer, as mentioned above. The cooling analysis is greatly important in PIM because thermal conductivity of PIM feedstock is much higher than for a common plastic, so the slip layer plays a significant role as an insulator.

Demonstration of Usefulness and Optimization

This section presents simulation results from some of the 2.5D examples to demonstrate the usefulness of the CAE analysis and optimization capability of the PIM injection molding process. We have shown that the developed CAE tool for PIM process is capable of predicting the filling pattern, temperature distribution, clamping force, and other important variables. We will demonstrate how to use this basic information from the simulation tool to predict injection molding related defects and will present the systematic way of using the CAE tool to develop an optimal injection molding process.

Basic Capability: Short Shot, Flash, Weldline, Air Vent, and Other Features

This section will demonstrate use of the simulation results to predict typical molding defects. There are many kinds of molding defects and we can identify them mainly as basic defects, dimensional defects, and other defects. The basic defects are traced to the molding parameters.

For the basic defects, simulations use the pressure field analysis to predict short shots and flashing, as well as the filling pattern to identify trapped air and weld line location. A short shot occurs when the molded part is filled incompletely because insufficient material was injected into the mold. Several factors cause the short shot defect, such as an insufficient-sized or restrictive flow area, low melt

temperature, low mold-wall temperature, a lack of vents, low injection pressure, and premature solidification. By using computer simulations, short shot defects is predicted and minimized by analyzing the mold filling pattern from the pressure, velocity, and temperature results. Flash is a defect where excessive material is found at locations where the mold separate, notably the parting surface, moveable core, vents, or venting ejector pins. The causes of flash are low clamping force, gap within the mold, molding conditions, and improper venting. Flash is avoided by using the clamping force calculation results and from the simulation results. Figure 8 shows the example of short shot and flash of PIM component.

Weldline and the resulting mark or knit line is another flaw that is also a potential weakness in a molded plastic part. Weldlines are formed by the union of two or more streams of feedstock flowing together, such as when flow passes around a hole, insert, or in the case of multiple gates or variable thickness in the component. Consequently, a weldline reduces the strength of the green component and leaves an undesirable surface appearance and should be avoided when possible. The results from the computer analysis are used to predict the weldline location. Air trap or air vent is a defect by air that is caught inside the mold cavity. The air-trap locations are usually in areas that fill last. The air-trap is predicted from the filling pattern analysis and be avoided by reducing the injection speed, enlarging or properly placing vents. Figure 9 shows predicted location of short shot, air trap and weld line from the injection molded PIM components.

Other defects, such as burn marks, flow marks, meld lines, jetting, surface ripples, sink marks, and such are also accessible using computer simulation tools in the design process stage. Especially important in production are control of factors related to dimensional uniformity. These are analyzed by checking all three main stages of the injection molding. Good component quality with uniform mass and uniform green density is important to hold final dimensional control. Table 5 is an example of the solution windows used to drive PIM towards dimensional stability during each stage of PIM.

Imbalanced Filling of Multiple Cavity Tooling

By increasing the number of quality components produced during a given molding cycle (multi-cavity molds), the cost of tooling increases yet the cost of production is reduced. This assumes that each component produced in each cavity of the multi-cavity mold will be identical. However, despite almost identical cavities, flow paths, cooling, and other control parameters, variations often exist between molded components. These variations significantly limit the benefit of a multi-cavity mold. Using computer simulations allows for balancing of the multiple cavity filling event. Firstly, from the cooling analysis, the cooling channel is configured to obtain a uniform mold wall temperature around each component. Secondly, from the 3D delivery system, by analyzing the conduction effect of the flow in

each branch, the delivery system is appropriately configured. Combining these results with a viscous heating analysis leads to optimization of the processing variables, as well as cavity design and delivery system and cooling channel design.

Figure 10(a) shows the FEM meshing for a eight cavity delivery system. Figure 10(b) visually shows the filling difference associated with a shift in the mold filling time. In this case slightly slower filling was beneficial.

Figure 11(a) shows the cooling analysis and temperature difference in two neighboring cavities. The difference in temperature distributions in the two cavities result from the combination of the cooling channel configuration and the viscous heating effect in the delivery channel.

Balanced Filling

Flow balancing during filling in a multiple cavity tool set requires understanding of the melt front velocity (MFV) and melt front area (MFA) profiles. As the name suggests, MFV is the melt front advancement speed and MFA is the cross-sectional area advancement, and is either the length of the melt front multiplied by the thickness of the component, the cross-sectional area of the runner, or a sum of both, if the melt is flowing in both places. At any time, the product of local MFV and MFA along all moving fronts is equal to the volumetric flow rate [22-23];

$$\text{MFV} \equiv \frac{Q}{\text{MFA}} \quad (18)$$

where Q is the volumetric flow rate. A high feedstock velocity at the melt front gives a higher surface stress with more molecular orientation and particle migration. A variable velocity of the melt front during filling results in differential sintering shrinkage and component warpage. Therefore, it is desirable to maintain a constant velocity at the melt front to generate uniform molecular orientation and minimized particle migration in the flow direction (not in thickness direction), which results in uniform material properties. Therefore, MFV and MFA are important design parameters, especially for balancing the flow during cavity filling. For example, MFA is used to quantitatively compare the degree of flow balance.

Figure 12 illustrates MFV and MFA variations in plate component that has four gates. Due to the variable gate locations and filling pattern, a constant MFV is not guaranteed even with a constant volumetric flow rate (or equivalently, a constant ram speed). Portions of the melt front reach the end of the cavity while other portions are still moving. We will discuss about optimizing the ram speed profile or relocation of gate location by minimizing the MFA in the cavity at the ‘Optimization’ section.

Sensitivity Analysis

Simulating and optimizing the powder injection molding process is difficult since several material, component, and process parameters are linked. It is difficult to identify critical parameters in the computer design owing to the fact that multiple objective functions have to be considered. An important question arises pertaining to how variations in material property influence the errors arising in predictions of various simulated parameters. During the design of a component, adjustment is made to its size to improve the functional and aesthetic attributes of the component. Additionally, changes are made to the location and dimensions of the melt delivery system to improve the manufacturability of the component. These issues also raise questions as to how small changes in dimensions influence process variations. Finally, several process settings are controlled by the operator on the injection molding machine during the production stage. It is important to understand how a computerized design tool captures the influence of such process variations in its prediction. [22]

Process, design, and material parameters is optimized using sensitivity analysis. It is a valuable tool for the design engineer determining the critical input parameters, as well as for the production engineer who has to optimize production. For the sensitivity analysis, the input parameters are varied over a fixed range (for example, $\pm 5\%$) and the response of the output parameters is monitored. The sensitivity is calculated as the slope of the dimensionless dependent variable with respect to the dimensionless independent variable, according to the following equation:

$$\text{Sensitivity} \equiv \frac{\text{percentage change in output}}{\text{percentage change in input}} \equiv \frac{\text{increment in output/initial value of output}}{\text{increment in input/initial value of input}} \quad (19)$$

This definition of sensitivity was used to compare input and output parameters having different dimensions. For example, a sensitivity value of -1.5 means that the percentage decrement of output is 1.5% if the percentage increment of input is 1.0%. It is independent of input and output parameters units. The result from Atre *et al.* [22] is shown in Figure 13, showing all normalized sensitivity values between the input and output parameters, which means that both the pressure related and temperature related output parameters are sensitive to process conditions, geometry conditions and feedstock properties, while the flow related output parameters are sensitive to the process and geometry conditions. The abbreviations used for the Figure 13 are as follow:

For classification of input parameters,

- PC (Processing Conditions): filling time (t_f), switch over point (SO), injection temperature (T_i), and mold wall temperature (T_w)

- GC (Geometry Conditions): part thickness (PT), gate diameter (GD), runner diameter (RD), and sprue diameter (SD)
- FP (Feedstock Material Properties): density (ρ), specific heat capacity (C_p), thermal conductivity (k), transition temperature (T_g), eject temperature (T_e), viscosity parameters (n, B, C, T_b, τ_y)
- BP (Binder Material Properties): density (ρ_b), specific heat capacity ($C_{p,b}$), thermal conductivity (k_b), viscosity parameters ($B_b, T_{b,b}, \beta, m$)

For classification of output parameters,

- Pressure-related: injection pressure (P_i), clamping force (f_c), and maximum shear stress (τ_{max})
- Temperature-related: Melt front temperature difference (ΔMFT), packing time (t_p), and cooling time (t_c)
- Velocity related: maximum shear rate ($\dot{\gamma}_{max}$), average MFV (μMFV), standard deviation of MFV (σMFV), average MFA (μMFA), standard deviation of MFA (σMFA).

Optimization 1: Filling Time

Filling time is an important variable that is optimized to reduce the required injection pressure. From the CAE filling analysis, by varying the filling time the injection pressure is calculated. When plotting the required injection pressure versus various filling times, the optimal filling time ranges are determined for the lowest injection pressure. The curve is U-shaped because, on the one hand, a short fill time involves a high melt velocity and thus requires a higher injection pressure to fill the mold. On the other hand, the injected feedstock cools more with a prolonged fill time. This results in a higher melt viscosity and thus requires a higher injection pressure to fill the mold. The shape of the curve of injection pressure versus fill time depends very much on the material used, as well as on the cavity geometry and mold design. If the required injection pressure exceeds the maximum machine capacity, the process conditions or runner system must be modified. Figure 14 (a) and (b) show the optimum filling time selection for the selected multi-cavity mold.

Optimization 2: Gate Location and Number of Gates

For a given component geometry, a filling analysis is generated based on the filling patterns from the first case of Figure 15, we can reduce the injection molding pressure by trying other location for the gate from single end to single center location. Based on the new gate location, the injection pressure is calculated. Compared to the previous design, the injection pressure is reduced. Further reduction of the injection pressure can be obtained by using multiple gates. With the three gates evenly distributed along the diagonal direction, the injection pressure reduced from 24.2 MPa for the single end gate to 6.29 MPa.

Optimization 3: Delivery System and Ram-Speed Profile

Figure 16(a) shows the meshed geometry and solid layer fraction distribution of a cellular phone housing

with a center gate and Figure 16(b) shows the corresponding optimal ram-speed profile that minimizes the MFV based on the current gate location. Table 6 shows that all other variables are also have been improved due to this delivery and ram-speed profile optimization.

Optimization 4: Design of Experiments

There are many injection molding parameters that affect green component properties. Therefore, a design of experiment (DOE) approach is used where there are many inputs. The most frequently used methods are partial or full fractional design and the Taguchi approach [18, 24]. If an appropriate DOE method is used, one can easily establish whether the inputs have an effect on the outputs of the system. We will demonstrate an optimization study for the multi-cavity shown in Figure 14. Taguchi method follows this procedure,

- Determine the objective function to be optimized
 - minimize weight of delivery and injection pressure
- Identify the control factors and their levels
 - injection temperature (A),
 - mold wall temperature (B),
 - diameter of main runner (C), and
 - diameter of branched runner (D),
- Identify constraints
 - capability of injection molding machine is constraints
- Design the matrix experiment and define the data analysis procedure
 - L_9 (3^4) Orthogonal array
- Predict the performance at these levels
 - simulation or experiment based on L_9 array
- Analyze the data and determine optimum levels for control factors
 - the larger the signal to noise ratio the better
- Conduct the matrix experiment.

The four input parameters (injection temperature, mold-wall temperature, diameter of main runner, and diameter of branched runner) are the control factors and the optimization procedure involves the determination of the ‘best’ levels of control factors. The ‘best’ levels of control factors are those that maximize the ‘signal-to-noise (S/N)’ ratios. Maximizing the S/N ratio results in the minimizing of any property which is sensitive to noise. We choose ‘the-larger-the-better’ characteristic of the S/N ratio because a high value of S/N implies that the signal is higher than the uncontrollable noise factors. The S/N ratios were calculated using equation which is measured in unit decibels (db),

$$S/N = -\log_{10}[\text{mean sum of square of the measured data}] \quad (20)$$

The objective function need to be minimized is,

$$F = \alpha(\text{normalized weight of dilivery system}) + (1 - \alpha)(\text{normalized injection pressure}) \quad (21)$$

where α is an adjustable parameter selected by the user.

Table 7 depicts the Taguchi L_9 orthogonal array where 1, 2, and 3 represent low, medium, and high settings, respectively, and the results from the experiment. Figure 17 shows the S/N ratio analysis of the experiment. From the analysis, the total contribution of the injection temperature to the objective function is 47.22 %, mold wall temperature is 34.3 %, diameter of main runner is 12.42 %, and diameter of branch is 6.06 %.

The conditions corresponding to No.9 proves optimal, and the combination minimizes the objective function when the injection temperature as 140 °C, mold wall temperature 45 °C, diameter of main runner as 5 mm, and diameter of branch runner as 4 mm are the combination getting the scrap saving 24 % and reduction of the injection pressure 0.1 % from the initial design.

Summary

This article shows the unique attributes for powder injection molding filling simulations. After molding, assuming the component is rigid, then the components are subjected to a heating cycle where both binder burnout and sintering take place. The constitutive models for sintering are covered in Section 9A.

However, for the PIM components the sintering shrinkage is large, since the compact starts near 60% dense and shrinks about 15% in attaining a sintered density near 98% of theoretical. To date, simulations for the final size and shape are proving accurate. The current efforts are aimed at adding the debinding cycle onto the integrated molding and sintering simulations. This is obviously a topic for more research.

Acknowledgements

Considerable support in this simulation development was provided Young-Sam Kwon of CetaTech and Sundar Atre of Oregon State University.

References

1. R. M. German and A. Bose, *Injection Molding of Metals and Ceramics*, Metal Powder Industries Federation, Princeton, NJ, USA, 1997.
2. R. M. German, *PIM Design and Applications User's Guide*, Innovative Material Solutions, State College, PA, USA, 2003.
3. S. Kim and L. Turng, "Developments of three-dimensional computer-aided engineering simulation for injection molding," *Modelling and Simulation in Materials Science and Engineering*, vol. 12, 2004, pp 151-173.
4. C. J. Hwang and T. H. Kwon, "A full 3D finite element analysis of the powder injection molding filling process including slip phenomena," *Polymer Engineering and Science*, vol. 42, no. 1, 2002, pp 33-50.
5. K. Mori, K. Osakada, and S. Takaoka, "Simplified three-dimensional simulation of non-isothermal filling in metal injection moulding by the finite element method," *Engineering Computations*, vol. 13, no. 2, 1996, pp 111-121.
6. V. V. Bilovol, L. Kowalski, J. Duszczyk, and L. Katgerman, "Comparison of numerical codes for simulation of powder injection moulding," *Powder Metallurgy*, vol. 46, no. 1, 2003, pp 55-60.
7. C. Binet, D. F. Heaney, R. Spina, and L. Tricario, "Experimental and numerical analysis of metal injection molded products," *Journal of Materials Processing Technology*, vol. 164-165, 2005, pp. 1160-1166.
8. H. H. Chiang, C. A. Hieber, and K. K. Wang, "A unified simulation of the filling and post filling stages in injection molding. Part I: Formulation," *Polymer Engineering and Science*, vol. 31, no. 2, 1991, pp. 116-124.
9. C. A. Hieber and S. F. Shen, "A finite-element/finite-difference simulation of the injection molding filling process," *Journal of Non-Newtonian Fluid Mechanics*, vol. 56, 1995, p. 361.
10. T. H. Kwon and S. Y. Ahn, "Slip Characterization of Powder-binder Mixtures and its Significance in the Filling Process Analysis of Powder Injection Molding," *Powder Technology*, vol. 85, 1995, pp. 45-55.
11. S. J. Park and T. H. Kwon, "Sensitivity analysis formulation for three-dimensional conduction heat transfer with complex geometries using a boundary element method," *International Journal for Numerical Methods in Engineering*, vol. 39, 1996, pp. 2837-2862.
12. S. J. Park and T. H. Kwon, "Optimal Cooling System Design for the Injection Molding Process," *Polymer Engineering and Science*, vol. 38, 1998, pp. 1450-1462.
13. S. J. Park and T. H. Kwon, "Thermal and Design Sensitivity Analyses for Cooling System of Injection Mold, Part 1: Thermal Analysis," *ASME Journal of Manufacturing Science and Engineering*, vol. 120, 1998, pp. 287-295.
14. S. Ahn, S. T. Chung, S. V. Atre, S. J. Park, and R. M. German, "Integrated Filling, Packing, and Cooling CAE Analysis of Powder Injection Molding Parts," *Powder Metallurgy*, 2008, vol. 51, in

press.

15. D. M. Kalyon, "Apparent slip and viscoplasticity of concentrated suspensions," *Journal of Rheology*, vol. 49, 2005, pp. 621-640.
16. M. Rezayat and T. Burton, "A boundary-integral formulation for complex three-dimensional geometries," *International Journal of Numerical Methods in Engineering*, vol. 29, 1990, pp. 263-273.
17. M. Khakbiz, A. Simchi, and R. Bagheri, "Investigation of rheological behaviour of 316L stainless steel-2 wt-% TiC powder injection moulding feedstock," *Powder Metallurgy*, vol. 48, no.2, 2005, pp. 144-150.
18. B. Berginc, Z. Kampus, and B. Sustarsic, "Influence of feedstock characteristics and process parameters on properties of MIM parts made of 316L," *Powder Metallurgy*, vol. 50, no. 2, 2007, pp. 172-183.
19. P. Suri, R. M. German, J. P. de Souza, and S.J. Park, "Numerical Analysis of Filling Stage during Powder Injection Moulding: Effects of Feedstock Rheology and Mixing Conditions," *Powder Metallurgy*, vol. 47, no. 2, 2004, pp. 137-143.
20. M. Mooney, "Explicit formulas for slip and fluidity," *Journal of Rheology*, vol. 2, 1931, pp. 210-222.
21. M. L. Foong, K. C. Tam, and N. H. Loh, "Yield stress behaviour of metal injection moulding suspensions at elevated temperatures," *Journal of Materials Science*, vol. 30, 1995, pp. 3625-3632.
22. S. V. Atre, S. J. Park, R. Zauner, and R. M. German, "Process Simulation of Powder Injection Moulding: Identification of Significant Parameters during Mould Filling Phase," *Powder Metallurgy*, vol. 50, no.1, 2007, pp. 76-85.
23. L. S. Turng, *C-Mold Design guide – A resource for plastics engineers*, 3rd Ed., Advanced CAE Technology Inc., Troy, NY, USA, 1998.
24. R. Urval, S. Lee, S. V. Atre, S. J. Park, and R. M. German, "Optimization of Process Conditions in Micro Powder Injection Molding using Taguchi Robust Design Method: Part I. Primary Design Parameters," *Powder Metallurgy*, vol. 51, no. 2, 2008, pp. 133-142.
25. PIMSolver User's Guide, *Cetatech*, Ver. 2.0, 2005.
26. S. J. Park, S. T. Chung; A. Schenck, S. V. Atre, and R. M. German, "Avoiding Molding Defects During the PIM of 316L Stainless Steel," *Proceedings PIM 2003*, Innovative Material Solutions, State College, PA, USA, 2003.
27. C. J. Hwang, Y. B. Ko, H. P. Park, S. T. Chung, and B. O. Rhee, "Computer aided engineering design of powder injection molding process for a dental scaler tip mold design," *Materials Science Forum*, vol. 534-536, 2007, pp. 341-344.
28. C. Wu, S. V. Atre, S. Laddha, S. Lee, K. Simmons, S. J. Park, R. M. German, and D. T. Whyhchell, Sr., "Material Homogeneity in Powder Injection Molded Ceramic Microchannel Arrays," *PIM International*, vol. 2, no. 2, 2008, pp. 68-73.
29. S. V. Atre, S. J. Park, A. Schenck, T. G. Kang, and R. M. German, "Imbalance Filling of Multi-cavity

Tooling: A Comparison of Plastics and Metals,” *Proceedings PIM 2003*, Innovative Material Solutions, State College, PA, USA, 2003.

Table 1. Complete set of material properties of PIM feedstock with stainless steel powder 316L stainless steel (PF-15F, D_{50} :8.0 μm , Atmix Corp., Japan) combined with a wax-polymer based binder system at a solid volume of 53 %

property	PIM feedstock		binder system	
melt density	ρ_m	$3.98 \cdot 10^3 \text{ kg/m}^3$	ρ_b	$7.49 \cdot 10^2 \text{ kg/m}^3$
heat capacity	$C_{P,m}$	$6.85 \cdot 10^2 \text{ J/kg}\cdot\text{K}$	$C_{P,b}$	$2.29 \cdot 10^3 \text{ J/kg}\cdot\text{K}$
thermal conductivity	k_m	$1.84 \text{ W/m}\cdot\text{K}$	K_b	$0.178 \text{ W/m}\cdot\text{K}$
transient temperature	T_g	$52.8 \text{ }^\circ\text{C}$		
viscosity	B	$5.19 \cdot 10^{-3} \text{ Pa}\cdot\text{s}$	B_b	$5.72 \cdot 10^{-4} \text{ Pa}\cdot\text{s}$
	T_b	5370 K	$T_{b,b}$	3650 K
	n	0.180		
	τ^*	$6.37 \cdot 10^4 \text{ Pa}$		
	τ_v	100 Pa		
slip phenomena	velocity model		layer model	
	α_1	$5.42 \cdot 10^{-14} \text{ m/s}$	α_2	$2.73 \cdot 10^{-9} \text{ m}$
	β_1	$2.75 \cdot 10^{-2} / \text{K}$	β_2	$4.23 \cdot 10^{-3} / \text{K}$
	m_1	1.50	m_2	0.513

Table 2. PVT material properties of PIM feedstock with stainless steel powder 316L stainless steel (PF-15F, D_{50} :8.0 μm , Atmix Corp., Japan) combined with a wax-polymer based binder system at a solid volume of 53 %

parameter	solid	liquid
b_1	$2.190 \cdot 10^{-4} \text{ m}^3/\text{kg}$	$2.334 \cdot 10^{-4} \text{ m}^3/\text{kg}$
b_2	$7.716 \cdot 10^{-8} \text{ m}^3/\text{kg}\cdot\text{K}$	$1.156 \cdot 10^{-7} \text{ m}^3/\text{kg}\cdot\text{K}$
b_3	$1.000 \cdot 10^9 \text{ Pa}$	$2.940 \cdot 10^8 \text{ Pa}$
b_4	$1.000 \cdot 10^{-2} / \text{K}$	$4.689 \cdot 10^{-2} / \text{K}$
b_5	$3.450 \cdot 10^2 \text{ K}$	
b_6	$1.990 \cdot 10^{-7} \text{ K/Pa}$	
b_7	$1.446 \cdot 10^{-5} \text{ m}^3/\text{kg}$	
b_8	$3.388 \cdot 10^{-2} / \text{K}$	
b_9	$9.328 \cdot 10^{-9} / \text{Pa}$	

Table 3. Material properties for HP-13 tool steel as the water cooled mold material

material	property	value
HP-13 for mold	thermal conductivity	$1.05 \cdot 10^2$ W/m·K
water for coolant	density	974 kg/m ³
	Heat capacity	$4.20 \cdot 10^3$ J/kg·K
	thermal conductivity	0.688 W/m·K
	viscosity	$3.65 \cdot 10^{-4}$ Pa·s

Table 4. Processing conditions for 316L stainless steel U-shaped specimen

filling time	1 s
filling/packing switch over	98 %
packing time	5 s
packing pressure	13 MPa
injection temperature	120 °C
cooling time	10 s
coolant inlet temperature	20 °C
coolant inlet flow rate	50 cm ³ /s

Table 5 Relationship of variables to improve quality at each molding stage [25]

objective functions	design variables		
	filling stage	packing stage	cooling stage
minimum injection pressure	optimum filling time	optimum packing time to avoid backflow	
maximum productivity			optimum cooling time
minimum deformation	optimum ram-speed profile for uniform velocity at melt-front	optimum packing pressure for profile uniform shrinkage	optimum cooling system design for uniform and even cooling and eliminating hot spot

Table 6 Optimum filling stage scenario after the optimization (multi-cavity shown in Figure 14)

design parameters	initial	optimum
injection pressure	62.4 MPa	54.0 MPa (13.4 %)
clamping force	15.3 ton	13.2 ton (-13.7 %)
maximum shear stress	0.456 MPa	0.393 MPa (-13.8 %)
difference in melt front temperature (Δ MFA)	41.6 °C	9.8 °C (-76.4 %)
deviation of melt front velocity (σ MFV)	1411 mm/s	120 mm/s (-91.5 %)
solidification fraction	8.0 %	4.7 % (-41.4 %)

Table 7 the Taguchi L_9 orthogonal array used for the experiment and its result.

No.	$T_{injection}$ (°C)	T_{mold} (°C)	D_{main} (mm)	D_{branch} (mm)	Objective function	scrap (g)	pressure (MPa)
1	120	35	4.0	4.0	2.15	36.67	50.05
2	120	40	5.0	4.5	2.02	46.18	40.24
3	120	45	6.0	5.0	2.03	57.48	34.12
4	130	35	5.0	5.0	2.02	49.56	38.33
5	130	40	6.0	4.0	1.96	51.06	35.60
6	130	45	4.0	4.5	1.88	39.70	39.53
7	140	35	6.0	4.5	1.95	54.09	33.31
8	140	40	4.0	5.0	1.88	43.09	37.30
9	140	45	5.0	4.0	1.75	43.15	33.07
initial design	130	40	6.0	5.0	2.00	57.48	33.11

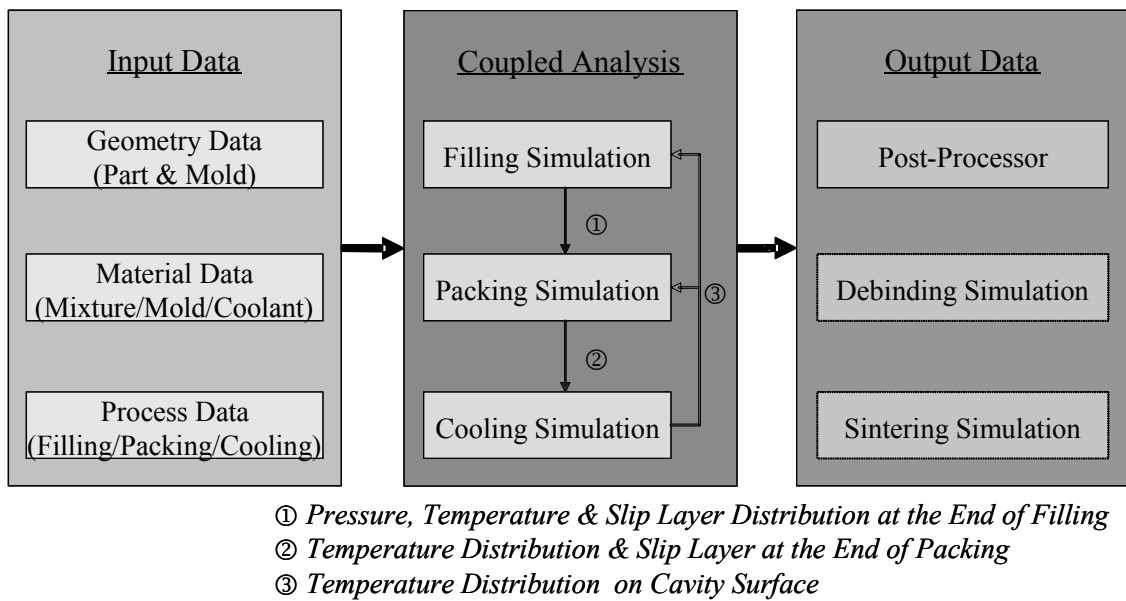


Figure 1. Overall structure of CAE Analysis of PIM Parts. [14]

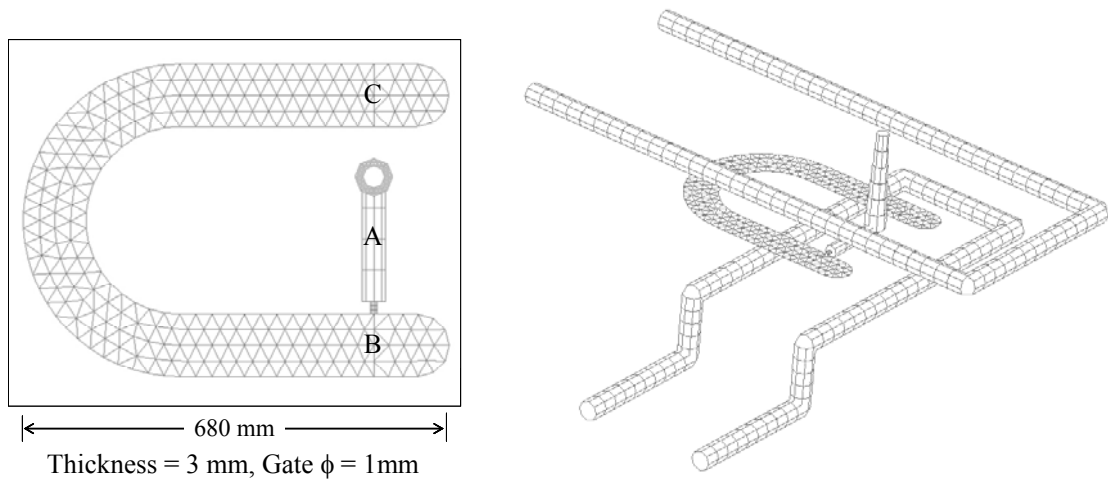
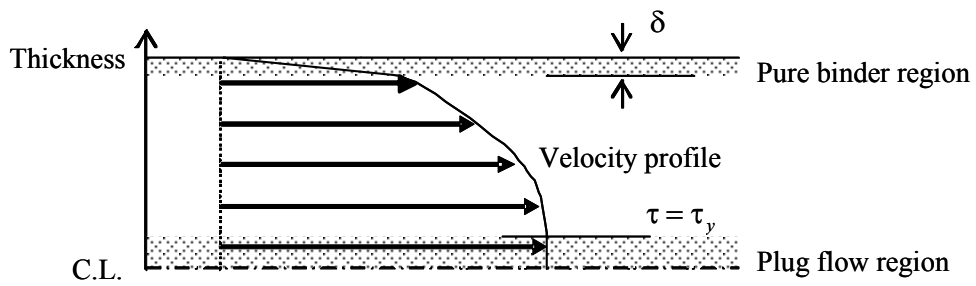
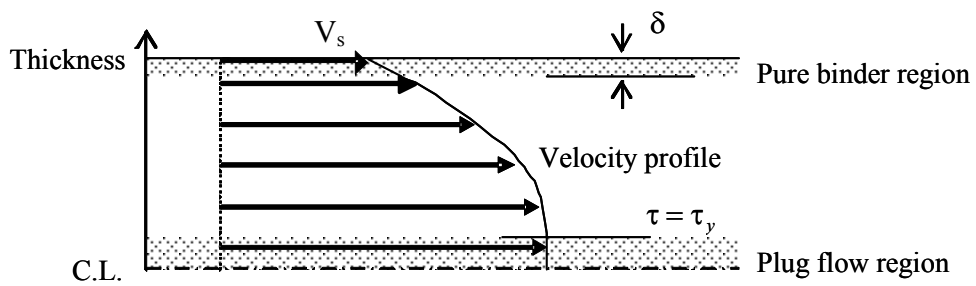


Figure 2. Geometry modeling and mesh generation for U-shape part including delivery system and cooling channels (Pressure measurements at A,B, and C). [14]



(a)



(b)

Figure 3. Schematic diagram of mold cavity filling flow with the slip layer model (a) and the slip velocity model (b) with yield stress. [10]

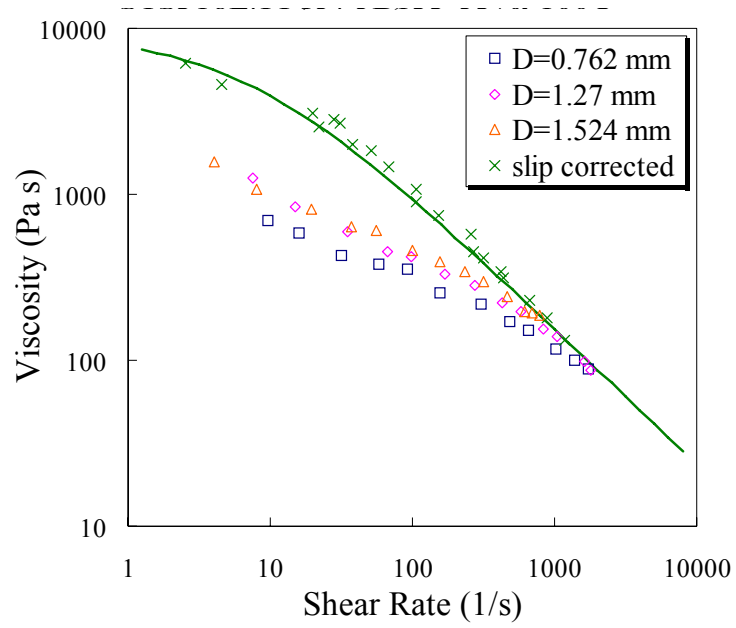


Figure 4. Slip corrected viscosity of the 316L stainless steel feedstock using three different capillary diameters [14]

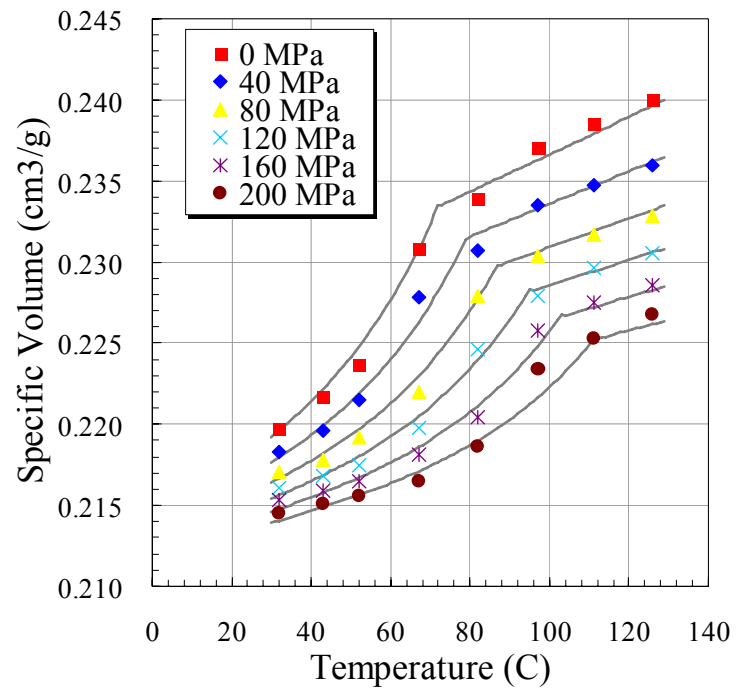
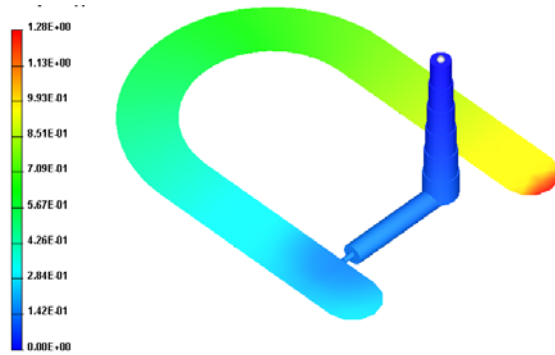
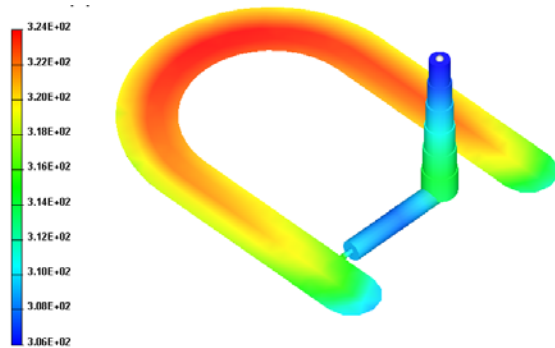


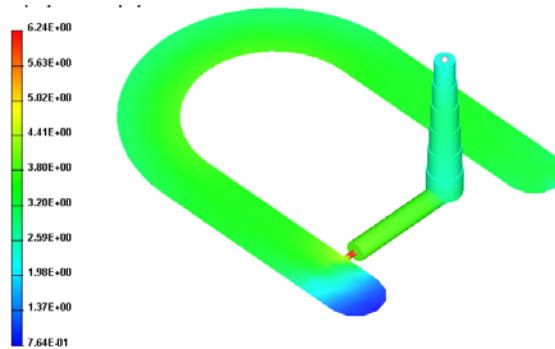
Figure 5. Pressure-volume-temperature (PVT) data of the feedstock [14]



(a) Filling pattern (Filling time 1.28 s)

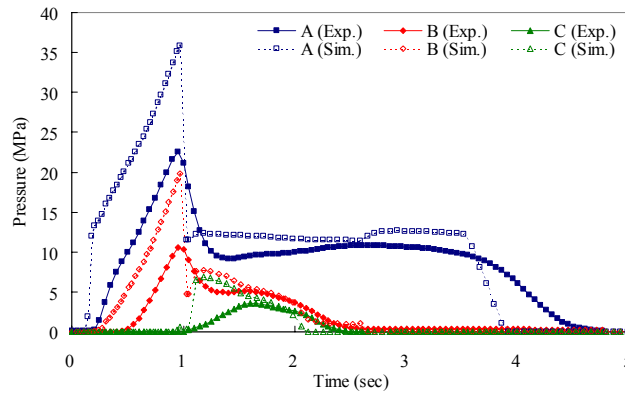


(b) Average mold cavity wall temperature distributions (K) between the upper and lower surfaces obtained from cooling analysis (maximum temperature = 51 °C and minimum temperature = 33 °C).

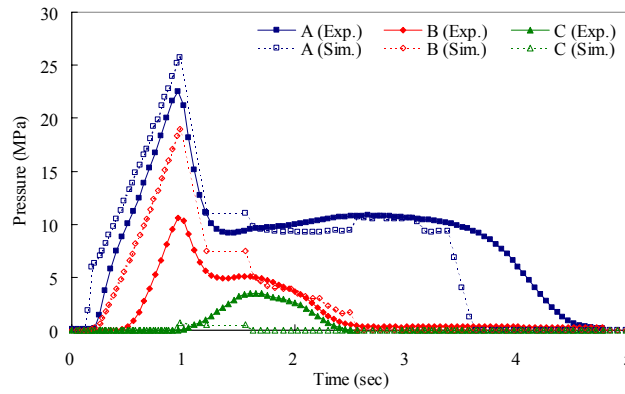


(c) Slip layer thickness distributions at the end of filling obtained from filling analysis (maximum thickness = 6.24 μm and minimum thickness = 0.76 μm).

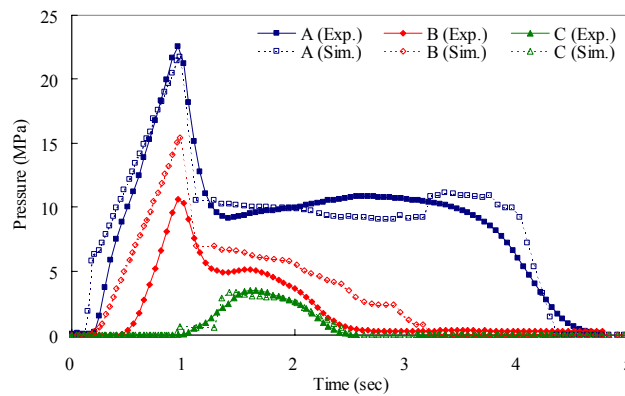
Figure 6. Simulation results with geometry input in Figure 2, material properties in Tables 1-3, and processing condition in Table 4. [14]



(a) without slip modeling and without interface with cooling analysis



(b) with slip modeling and without interface with cooling analysis



(c) with slip modeling and with interface with cooling analysis

Figure 7. Pressure-time plot at three points indicated in Figure 4. Simulation results are obtained from filling, packing, and cooling analyses with constant cavity wall temperature 30°C. [14]

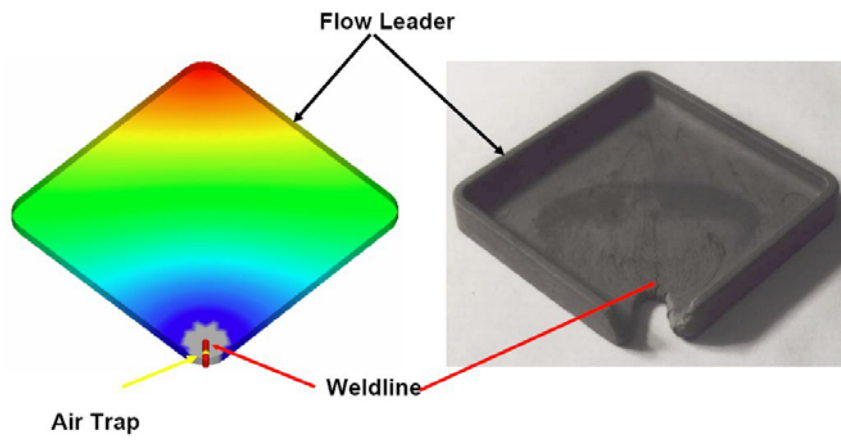


(a) Short shot

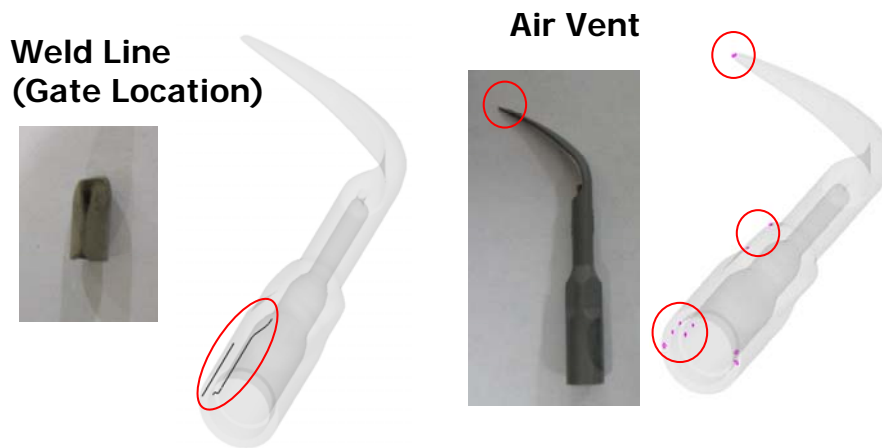


(b) Flash

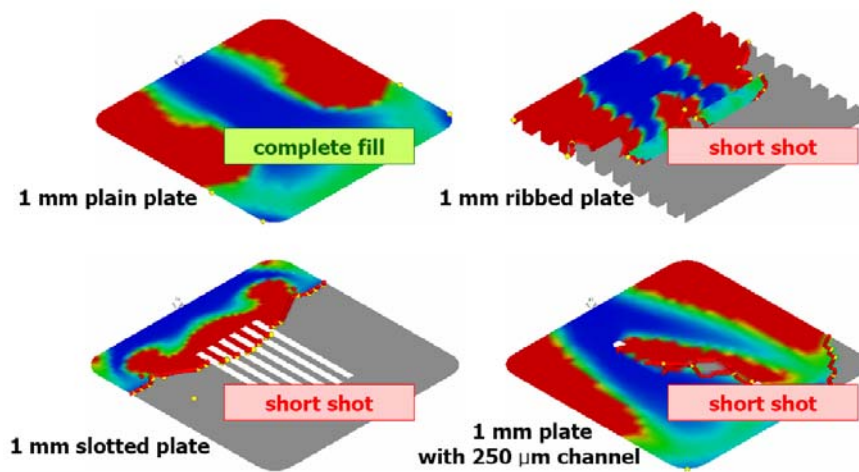
Figure 8. Short shot (a) is predicted by checking the filling pattern and flash (b) is avoided by clamping force calculation from the simulation results. [26]



(a) plate [26]

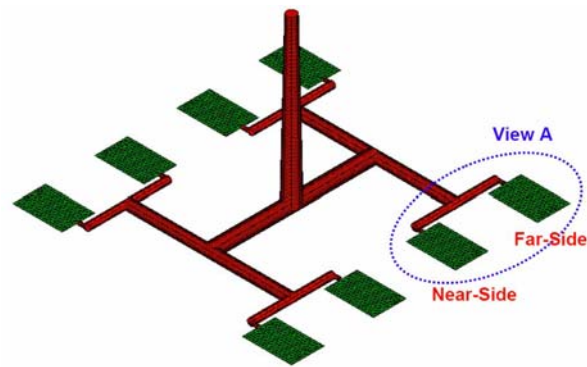


(b) dental scaler tip [27]



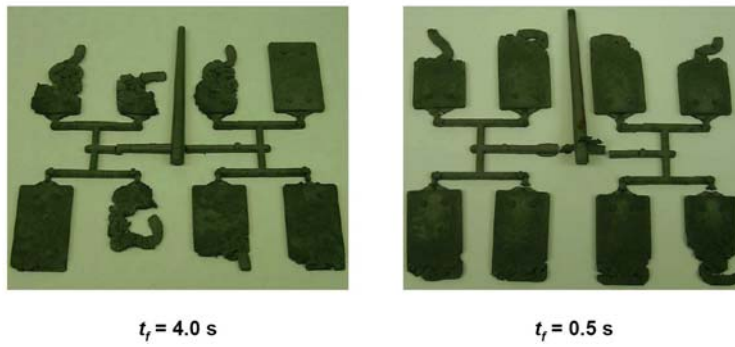
(c) geometry evaluation of micro features [28]

Figure 9. Weldlines and air trap/vent is predicted by using CAE tool for PIM process



(a)

Short-Shot Test with Various t_f



(b)

Figure 10 (a) FEM mesh for the multi-cavity and the delivery system and (b) Filling experiment showing the different filling pattern by changing the filling time (from 4.0 s to 0.5 s) [29].

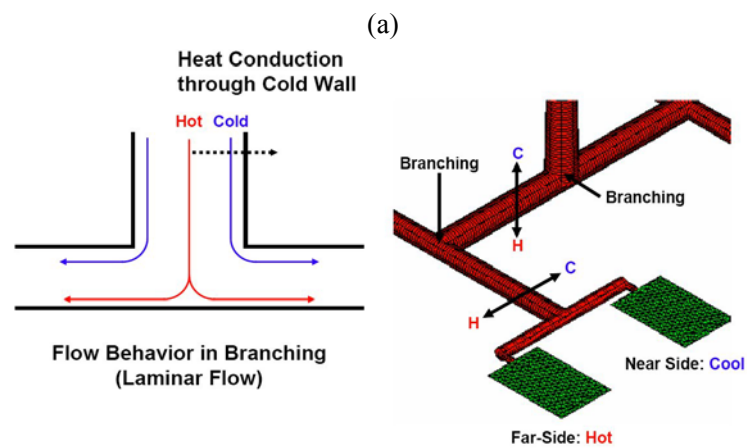
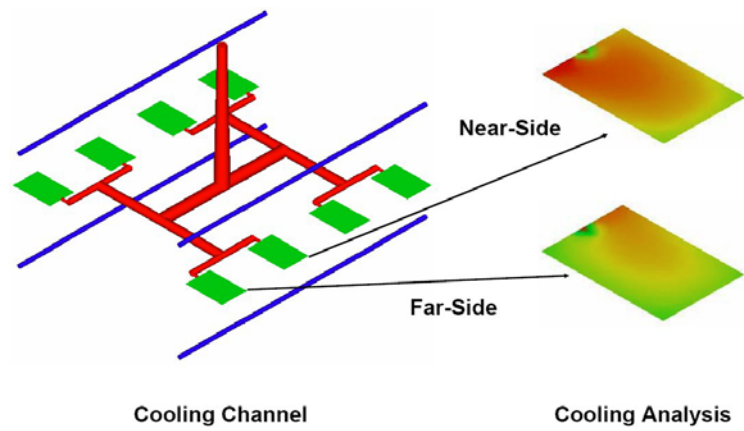
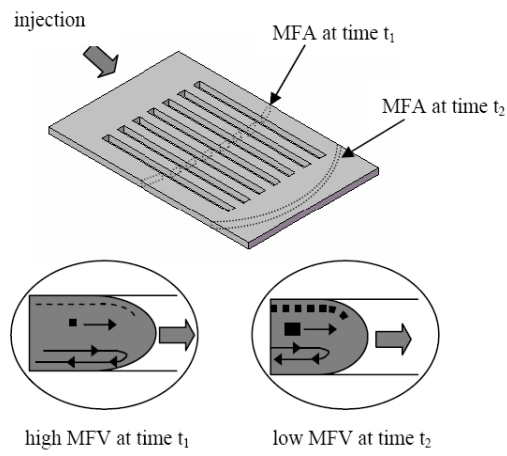
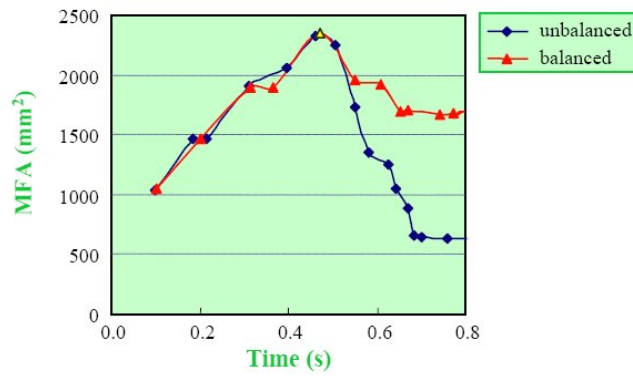


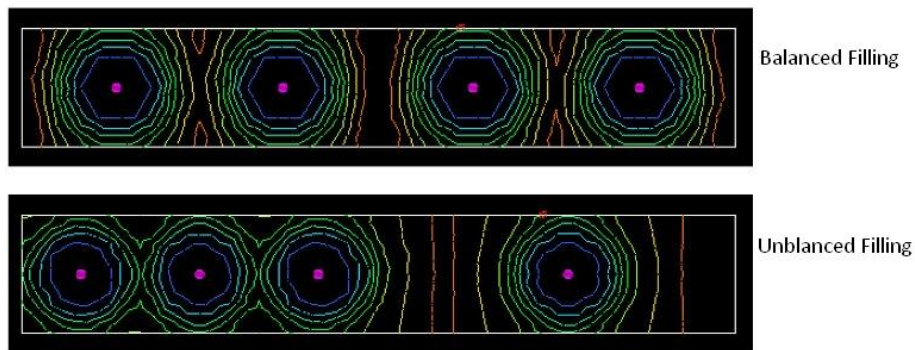
Figure 11 (a) A multiple cavity cooling analysis, showing the temperature difference in neighboring cavities due in what would appear to be a balanced flow system. The sketch in (b) illustrates how the viscous heating effect leads to this temperature imbalance [29].



(a)

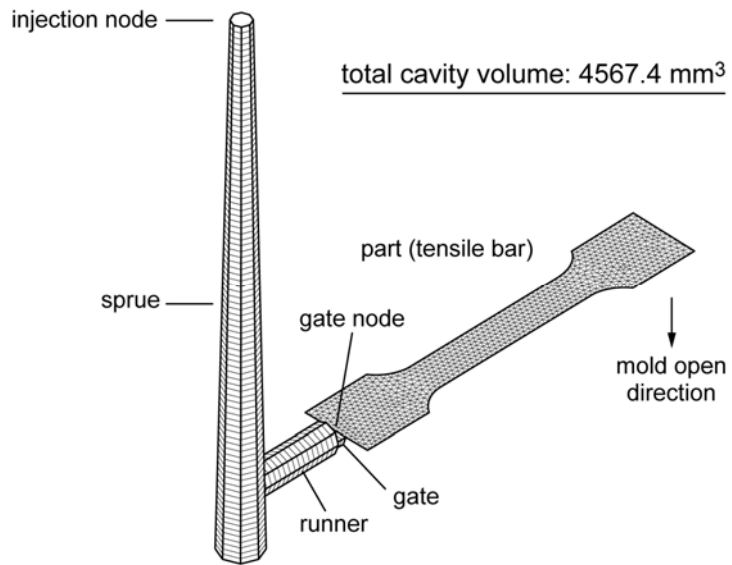


(b)



(c)

Figure 12 (a) Illustration of MFV and MFA, at t_1 , reduced MFA results high MFV and need to be adjusted by gate balancing or ram speed profile, (b) reduced MFA variation after gate balancing for the cavity of (c), and (c) variation in MFA and its corresponding filling pattern with balanced filling and unbalanced filling [25].

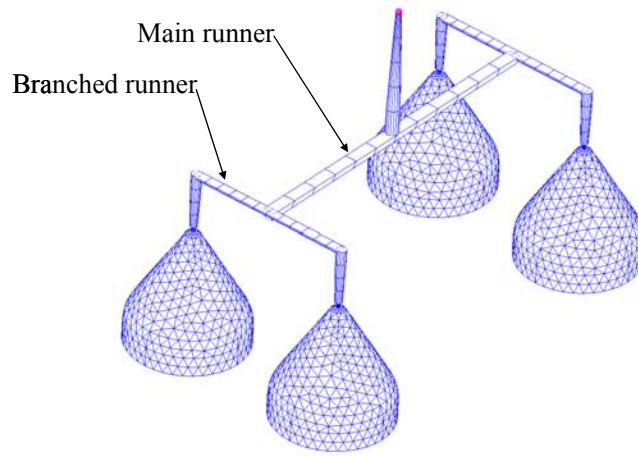


(a)

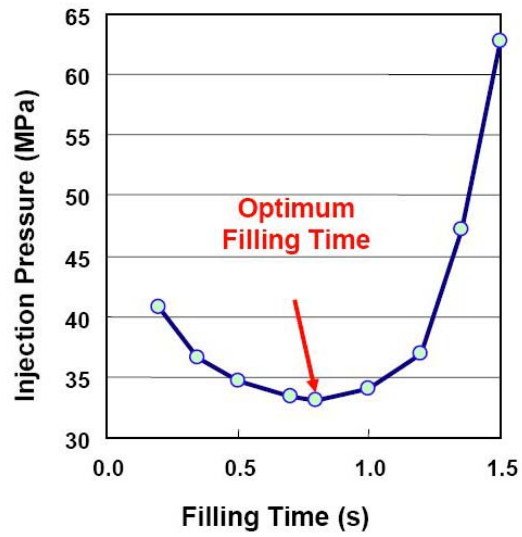
TENSILE BAR												
		PRESSURE-RELATED			TEMPERATURE-RELATED			FLOW-RELATED				
		P_i	f_c	r_{max}	ΔMFT	t_p	t_c	$\dot{\gamma}_{max}$	μ MFV	σ MFV	μ MFA	σ MFA
PC	l_r											
	SO	■	■	■	■	■	■	■	■	■	■	■
	\bar{T}_j	■			■	■	■				■	■
	T_w											
GC	FT	■	■	■	■	■	■	■	■	■	■	■
	GD	■			■	■	■	■	■	■	■	■
	RD											■
	SD											■
FP	ρ				■	■	■					
	c_p				■	■	■					
	k				■	■	■					
	T_g				■	■	■					
	T_e				■	■	■					
	n	■	■	■	■	■	■					
	β	■	■	■	■	■	■					
	C	■	■	■	■	■	■					
BP	P_D											
	$c_{p,b}$											
	k_b											
	B_D											
	$T_{3,b}$											
	α											
	β											
	m								■			

(b)

Figure 13. (a) Description of tensile components used for analysis, (b) Sensitivity analysis of output parameters towards input parameters for a tensile bar: solid is strong level, hatch medium level, and blank weak level. [22]

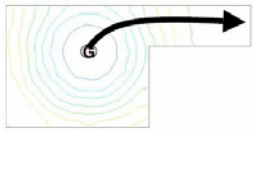
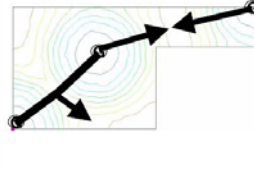


(a)



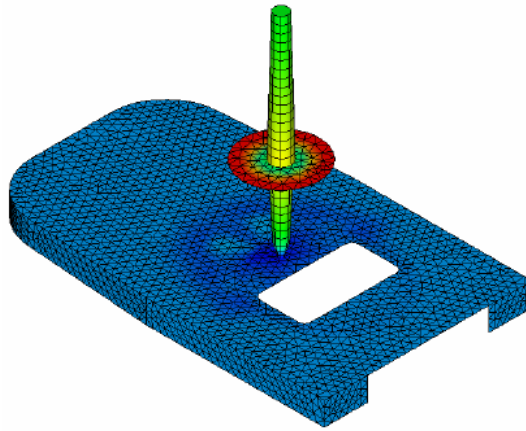
(b)

Figure 14 Filling time optimization by using CAE tool for PIM, (a) Mesh used for optimization study, (b) Optimum filling time finding which minimizes injection pressure [25]

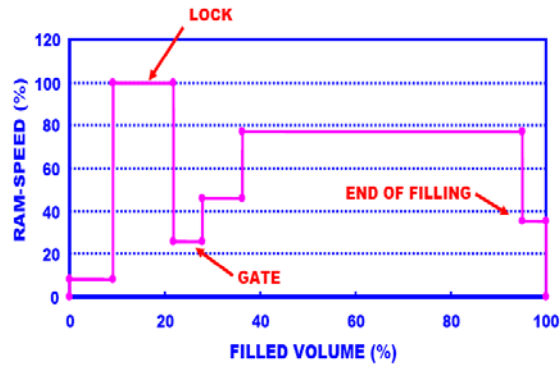
gate type	single end gate	single center gate	three gates
injection pressure	24.2 MPa	14.7 MPa	6.29 MPa
melt-front advancement and corresponding flow length			

(a)

Figure 15. Optimization of gate location and a number of gates [25]



(a)



(b)

Figure 16. Optimal ram-speed profile to maintain uniform MFV from the CAE simulation of cell phone shell application. (a) meshed geometry and (b) optimal ram speed profile which minimizes variation of MFV [26].

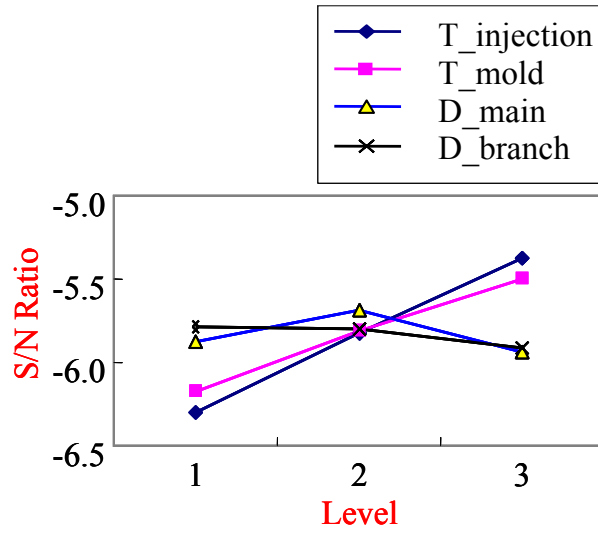


Figure 17. S/N Analysis of the multi-cavity showing that injection temperature is the most sensitive factor to achieve the objective function. [25]